

Article

Effect of Pole and Slot Combination on the AC Joule Loss of Outer-Rotor Permanent Magnet Synchronous Motors Using a High Fill Factor Machined Coil

Soo-Hwan Park ¹, Eui-Chun Lee ^{1,2}, Gi-Ju Lee ^{2,3}, Soon-O. Kwon ² and Myung-Seop Lim ^{1,*}

¹ Department of Automotive Engineering, Hanyang University, Seoul 04763, Korea; shwanp14@hanyang.ac.kr (S.-H.P.); 2chun@kitech.re.kr (E.-C.L.)

² Safety System R&D Group, Korea Institute of Industrial Technology, Daegu 42994, Korea; rrrww1211@kitech.re.kr (G.-J.L.); kso1975@kitech.re.kr (S.-O.K.)

³ Department of Electrical Engineering, Kyungpook National University, Daegu 41566, Korea

* Correspondence: myungseop@hanyang.ac.kr

Abstract: This paper proposes a design guideline for selecting the pole and slot combination of an outer-rotor permanent magnet synchronous motor (PMSM) using a maximum slot occupation (MSO) coil. Because the MSO coil has a large conductor area, the AC Joule loss in the conductors may be increased at high frequencies. To ensure high-efficiency for the PMSM, it is necessary to reduce the loss. Thus, it is important to select the pole- and slot- combination that has the minimum AC Joule loss. The loss is caused by skin/proximity effects and variations in the slot leakage flux. The skin effect is due to the armature winding and the variation in the slot leakage flux is due to the field flux. A method for separating the AC Joule loss due to each component using the frozen permeability method is proposed. Based on the proposed method, the effect of each cause on the loss at various pole- and slot- combinations is analyzed in this study.

Keywords: AC Joule loss; frozen permeability; MSO coil; outer-rotor; pole and slot combination



Citation: Park, S.-H.; Lee, E.-C.; Lee, G.-J.; Kwon, S.-O.; Lim, M.-S. Effect of Pole and Slot Combination on the AC Joule Loss of Outer-Rotor Permanent Magnet Synchronous Motors Using a High Fill Factor Machined Coil. *Energies* **2021**, *14*, 3073. <https://doi.org/10.3390/en14113073>

Academic Editor: Anibal T. de Almeida

Received: 19 April 2021

Accepted: 22 May 2021

Published: 25 May 2021

Publisher's Note: MDPI stays neutral with regard to jurisdictional claims in published maps and institutional affiliations.



Copyright: © 2021 by the authors. Licensee MDPI, Basel, Switzerland. This article is an open access article distributed under the terms and conditions of the Creative Commons Attribution (CC BY) license (<https://creativecommons.org/licenses/by/4.0/>).

1. Introduction

Outer-rotor permanent-magnet synchronous motors (PMSMs) have been widely used as electrified powertrains (e-powertrains) in vehicle applications because of their high power density and efficiency [1,2]. Various studies have been conducted to improve the mileage of vehicles, which has been limited by the capacity of the batteries used as energy sources. To increase the mileage, the capacity of the batteries should be increased. However, this is not efficient because enlarging the battery capacity increases the weight of the vehicle [3]. It is more effective to improve the mileage by increasing the torque density and efficiency of PMSMs [4].

To improve the torque density, the fill factor of the stator winding should be increased. Over the past decades, the automotive industry has endeavored to improve the torque density and efficiency by increasing the fill factor of armature windings. As a result, winding technology using rectangular conductors such as hairpin windings has been developed [5–8]. The hairpin winding helps in achieving a higher fill factor than conventional round wires or flat wires, thus reducing the copper loss and increasing the torque density owing to the high current capacity [8]. However, the number of turns in a hairpin winding is limited by the structure of the end winding, and the hairpin winding has a critical disadvantage in that it cannot be used in concentrated winding machines. The maximum slot occupation (MSO) coil is a winding technology that increases the fill factor in concentrated winding machines, as shown in Figure 1 [9–11]. Because the MSO coil is manufactured by machining a copper block, it can be machined to fit into the slot shape. Therefore, the MSO coil enables an extremely high fill factor, thereby increasing the torque density and efficiency of the concentrated winding PMSM remarkably.

Because of the enlarged conductor area in the MSO coil, the AC Joule loss of the conductor should be considered when calculating the efficiency of the PMSM [12–14]. The loss occurs because of the armature and field magnetic flux and is proportional to the frequency of the magnetic flux [15]. The loss due to the armature magnetic flux is caused by the skin and proximity effect, which is in turn caused by eddy current flow in the conductor itself or in adjacent conductors. The loss due to the field flux is generated by the variation in the magnetic flux leaked into the slot. Because the AC Joule loss due to both causes is affected by the pole and slot combination, the loss for each cause should be analyzed in order to design a high-efficiency PMSM.

To analyze the AC Joule loss, it is necessary to separate the loss due to each cause. The total loss is generated by transient electromagnetic phenomena, including skin and proximity effects, and the variation in the slot leakage flux. The effects of these phenomena can be calculated using electromagnetic finite element analysis (FEA). The method of separating eddy current loss by each cause has been used to design high performance motors such as high-speed motors. In [16,17], rotors for ultra-high-speed motors have been designed by separating the eddy current loss of permanent magnets (PMs) by each cause using frozen permeability (FP) method. In this study, the method is used for separating the eddy current loss of conductors because the efficiency of motor using high fill factor winding is more affected by the eddy current loss of the conductor than the PMs. The FP method is a technique for linearizing a magnetic circuit by fixing the permeability of each element using the results of FEA nonlinear electromagnetic analysis [18,19]. Using the FP method together with electromagnetic FEA, it is possible to separate the eddy currents generated in the conductors by the armature current and the field magnetic flux. In this paper, a method for separating the loss by each cause using the FP method is proposed. In addition, the proposed method is used to analyze the variation in the loss with the pole and slot combination.

The contributions of this study are as follow. First, we propose a guideline for selecting optimal pole and slot combinations with low AC Joule loss, in the case of applying high fill factor winding. Second, in order to analyze the AC Joule loss according to the number of poles and slots, a method of separating the loss using FP method is used. It is expected that a high-power, high-efficiency motor can be designed with the proposed method.

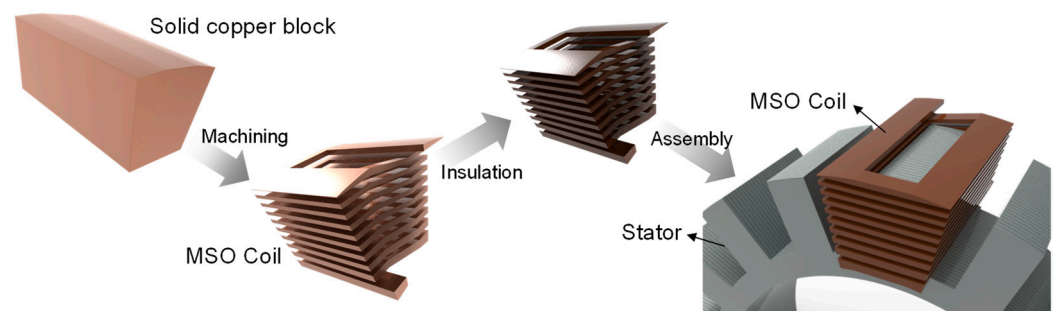


Figure 1. Manufacturing process of MSO coil.

2. Investigation of AC Joule Loss

2.1. Causes of the AC Joule Loss in Armature Conductors

AC Joule loss in armature conductors occurs because of two factors. The first is the skin and proximity effect of the AC flowing through the armature winding, as shown in Figure 2a. The AC flowing in the conductor itself or adjacent conductors changes the magnetic field and generates an induced voltage. The eddy current caused by the induced voltage causes a skin effect and a proximity effect, leading to an imbalance in the current density in the conductors that increases the Joule loss in the conductors.

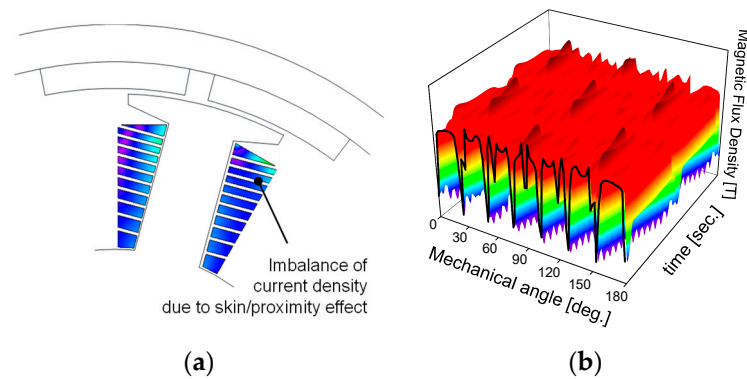


Figure 2. Causes of AC Joule loss. (a) Skin and proximity effect due to armature AC and (b) variation in slot leakage flux.

The second cause of the loss is the variation in the slot leakage component of the field magnetic flux, as shown in Figure 2b. As the rotor rotates, the space and time harmonics of the slot leakage flux combine to produce asynchronous field components relative to the conductors that induce eddy currents in the conductors, causing an imbalance in the current density in the conductors. Every procedure using electromagnetic FEA were performed using a commercial FEA software JMAG, and the AC Joule loss of the conductor was calculated using 2D electro-magnetic transient analysis. The AC Joule loss was analyzed by applying sinusoidal current to exclude the effect of PWM voltage.

2.2. AC Joule Loss Separation Using Frozen Permeability Method

It is necessary to separate the AC Joule loss due to each component to analyze the effect of the pole and slot combination on the loss. The loss can be calculated using electromagnetic FEA as:

$$W_{AC} = \frac{1}{\sigma} \int \mathbf{J} \cdot \mathbf{J} dV \quad (1)$$

where W_{AC} and σ are the AC Joule loss and conductivity of each material, J is the current density, and V is the volume of the material. However, it is difficult to analyze the loss due to each cause because the skin/proximity effect and variation in the slot leakage flux are simultaneously considered when conducting the transient analysis. Therefore, a method of separating the loss due to each cause using the FP method is proposed, as shown in Figure 3. The flow of the proposed method is as follows:

- 1) Nonlinear electromagnetic FEA is performed to calculate the total AC Joule loss, $W_{AC,total}$. The permeability of each element is calculated considering the nonlinearity of the magnetic material.
- 2) Using the FP method, the magnetic circuit can be linearized by fixing the permeability of each element according to the result of the nonlinear FEA, as shown in Figure 4.
- 3) After linearizing the magnetic circuit, the variation in the slot leakage flux due to the PMs can be calculated by solving the magnetic circuit without an armature current. The AC Joule loss due to the variation in the slot leakage flux, $W_{AC,f}$ can then be calculated.
- 4) Because the total AC Joule loss is caused by the skin/proximity effect and the variation in slot leakage flux, the AC Joule loss due to the skin and proximity effect, $W_{AC,a}$ can be obtained by subtracting $W_{AC,f}$ from $W_{AC,total}$:

$$W_{AC,a} = W_{AC,total} - W_{AC,f} \quad (2)$$

Before using the proposed method to analyze the effect of the pole and slot combinations on the AC Joule loss, the method should be verified. To verify the method, the sum of the losses calculated using the FP method and the total loss was compared. The specimen

used for verification was a 14-pole and 12-slot outer-rotor PMSM. The specimen was one of the models used to analyze the effect of the pole and slot combination on loss due to each cause. Its specifications are listed in Table 1. Figure 5 shows the results of the verification of the proposed method at the rated torque at various rotation speeds of up to 2500 rpm. In this study, the AC Joule loss of the end winding is neglected and considered as DC Joule loss because the end winding is less affected by the radial flux path [8]. The DC Joule loss of the end winding was not considered in this verification. The differences between the sum of the AC Joule losses due to each cause calculated using the proposed method and the total loss is less than 0.1%. In addition, it can be seen that the increase in the loss with the rotational speed is mostly due to the variation in the slot leakage flux. Therefore, the proposed method can be used to separate the losses due to each cause.

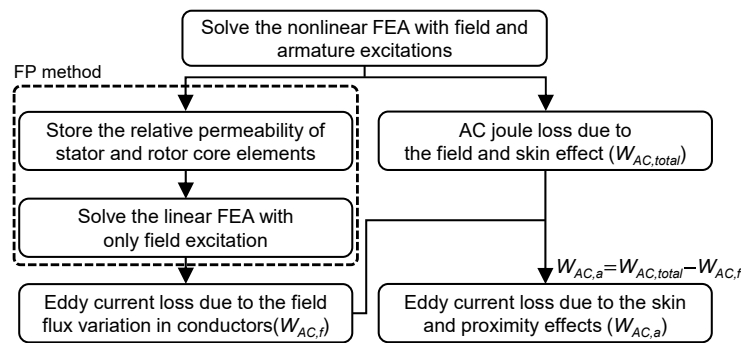


Figure 3. Process for separating AC Joule loss due to each cause.

Table 1. Specimen specifications.

Item	Unit	Value
Number of poles	-	14
Number of slots	-	12
Stator diameter	mm	80
Rotor diameter	mm	67
Stack length	mm	20.7
DC link voltage	V	48
Max. speed	rpm	2500
Rated torque	Nm	1.0
Permanent magnets	-	N38UH

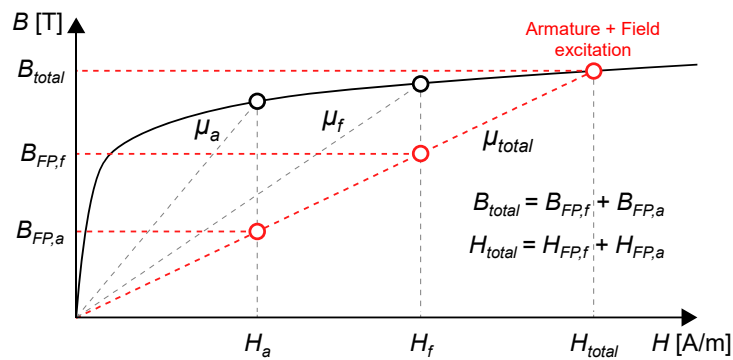


Figure 4. Principle of frozen permeability method for separating AC Joule loss.

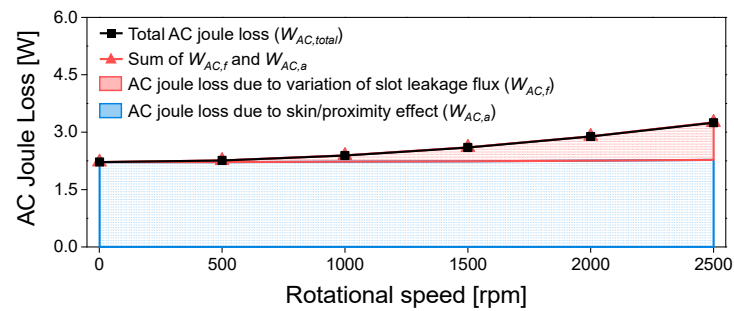


Figure 5. Verification of the proposed method.

3. Comparison of the AC Joule Loss According to the Pole and Slot Combination

3.1. Analysis Models

The increased current capacity resulting from the use of an MSO coil makes it possible to design a PMSM with high torque density suitable for the e-powertrain. However, the efficiency may be decreased by the increased AC Joule loss due to the enlarged conductor area. Therefore, it is necessary to analyze how the loss for each cause varies with the pole and slot combinations in order to design PMSMs that have high efficiency and torque density. The models used for analyzing the variation in the loss with the number of poles and slots are shown in Figure 6. These models were designed by adopting a design method that minimizes the magnetic reluctance of stator while maintaining important parameters such as pole arc of rotor [17,20]. To apply the MSO coil in the outer-rotor PMSM, pole and slot combinations with 8, 10, and 14 poles and 12, 15, and 18 slots, which allow concentrated winding, were selected. Each model was designed to have the same inner and outer diameters of the stator/rotor and air-gap length, as shown in Table 1, as well as the same back electromotive force (back-EMF) so that comparisons could be made under the same conditions. The winding factors of each pole and slot combination are shown in Figure 6. Because the winding factors for each model were different, MSO coils with different numbers of turns were designed to generate the same back-EMF. The variation in the AC Joule loss with the rotational speed at the rated torque of 1 Nm is compared.

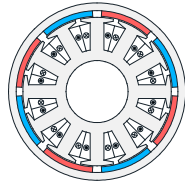
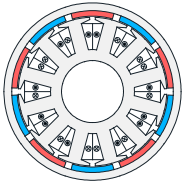
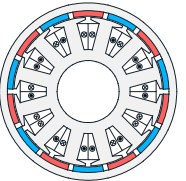
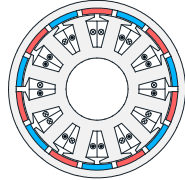
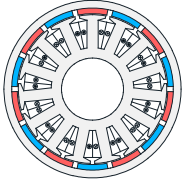
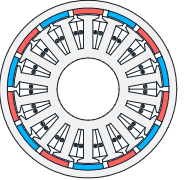
Models for verifying the effect of rotor poles				
	8-poles 12-slots	10-poles 12-slots	14-poles 12-slots	
	Winding factor (1st)	0.866	0.933	0.933
	Series turns per phase	64	52	44
Conductor area [mm ²]	1.27	1.77	2.25	
Models for verifying the effect of stator slots				
	14-poles 12-slots	14-poles 15-slots	14-poles 18-slots	
	Winding factor (1st)	0.933	0.951	0.902
	Series turns per phase	44	45	54
Conductor area [mm ²]	2.25	2.33	1.90	

Figure 6. Analysis models for analyzing the effect of rotor poles and stator slots on the AC Joule loss.

3.2. Trend of AC Joule Loss According to the Number of Poles

Figure 7a,b show the analysis results of the AC Joule loss at various numbers of poles. The fundamental frequency increased with the number of poles. Therefore, the frequencies of the armature current and slot leakage flux increased as well, leading to corresponding increases in the skin and proximity effect and eddy current loss due to slot leakage flux variation. However, the total loss decreased as the number of poles increased, as shown in Figure 7a. This is because the series turns per phase of the models with low winding factors were increased to maintain the back-EMF at the same rotational speed. The Joule loss due to the armature current therefore increased with the number of series turns per phase because of the increased length of the conductor and the reduced conductor area. In addition, the eddy current loss generated by the slot leakage flux variation decreased as the number of series turns per phase increased owing to the reduced conductor area. Consequently, the total loss decreased as the number of poles increased because the contribution of the armature current to the loss was much larger than that of the slot leakage flux, as shown in Figure 7b. In addition, the total loss at different rotational speeds was highly affected by the variation in the slot leakage flux, as shown in Figure 7b. Therefore, the AC Joule loss at different frequencies was more affected by the field flux than by the skin and proximity effect.

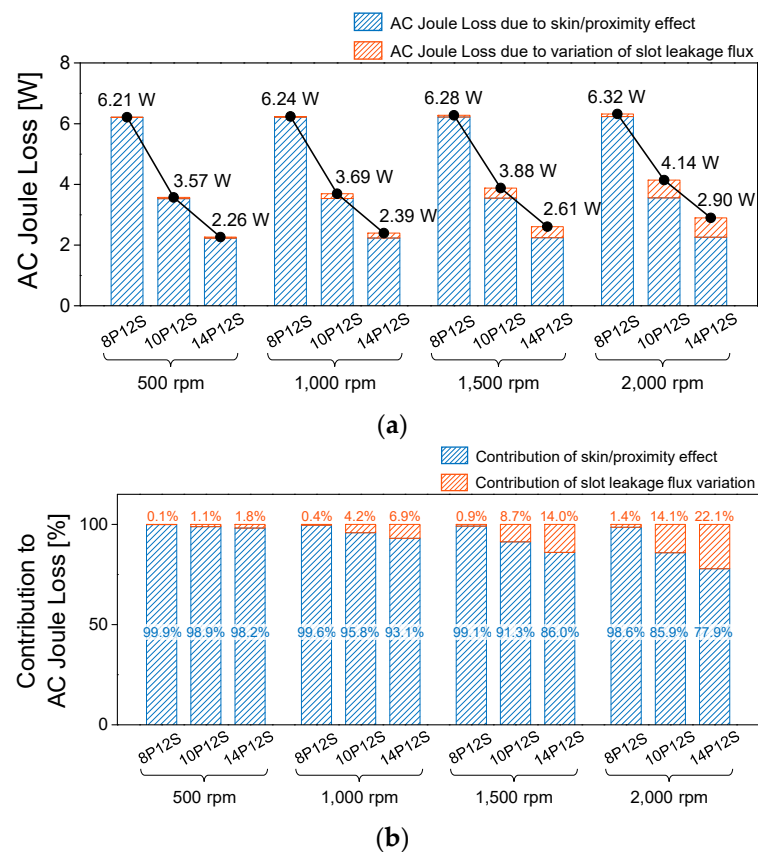


Figure 7. Effect of rotor poles on AC Joule loss. (a) AC Joule loss and (b) contribution to AC Joule loss by each cause at various numbers of poles and rotational speeds.

3.3. Trend of AC Joule Loss According to the Number of Slots

Figure 8a,b show the analysis results of the AC Joule loss at various numbers of slots. Because the frequency of the slot leakage flux was proportional to the number of slots, the loss due to the slot leakage flux increased with the number of slots. In addition, the Joule loss due to the armature current increased because of the increased number of series turns per phase to maintain the same back-EMF. Consequently, the total loss increased with

the number of slots, as shown in Figure 8a. In addition, the loss at each frequency was more affected by the field flux than the skin and proximity effect, as shown in Figure 8b. This trend is similar to the results when the number of poles was fixed. However, the differences between the proportions of the armature current and field flux on the AC Joule loss at different slot numbers were similar. This is because the differences between the series turns per phase at different number of slots were not large because the winding factors were similar.

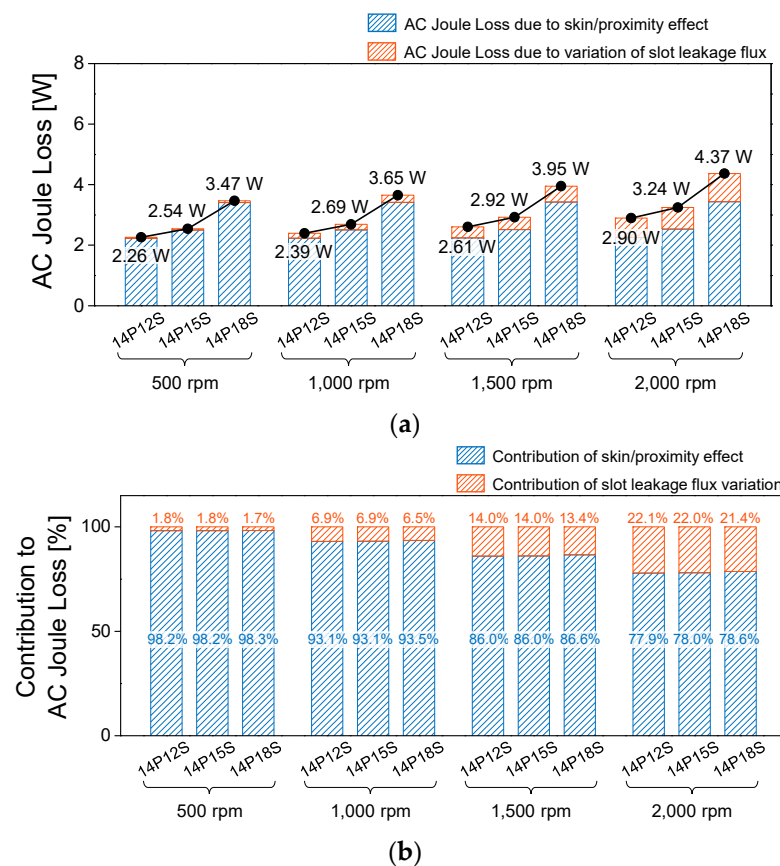


Figure 8. Effect of stator slots on AC Joule loss. (a) AC Joule loss and (b) contribution to AC Joule loss by each cause at various numbers of poles and rotational speeds.

Based on the analysis of the AC Joule loss at the various pole and slot combinations, the combination of 14 poles and 12 slots, which had the lowest AC Joule loss under the rated torque, was selected as the pole and slot combination of the PMSM to be used for the e-powertrain.

4. Experimental Verification

In this section, the experimental results for a specimen with 14 poles and 12 slots are compared with the simulation results. Figure 9a shows the manufactured MSO coil and assembled PMSM. After the machined MSO coil was insulated, it was assembled with the stator to complete the PMSM. To investigate the mechanical loss in the simulations, experiments were conducted using a dummy rotor manufactured using the non-magnetized material S45C, as shown in Figure 9b. The mechanical loss can be measured using the dummy rotor because there is no electromagnetic loss resulting from field excitation in the stator core and armature winding. The procedure for measuring the mechanical loss is as follows [10]. To exclude the effect of the temperature variation, the experiments were conducted after rotating the specimen for 30 min. Then, a servo motor for driving the specimen is controlled with constant speed. The mechanical power which is for driving the specimen with constant speed is measured. The mechanical power can be calculated as

the product of the torque measured from the torque sensor and the rotational speed. Then, the mechanical loss is equivalent to the measured mechanical power. The abovementioned experiment is performed repeatedly according to the rotational speed. Figure 9c shows the experimental setup for measuring the mechanical loss and efficiency of the specimen. The experiment was conducted at the rated torque of 500–2000 rpm. Figure 10 shows the results of the mechanical loss measurement. The mechanical loss is caused by friction in the fluid of the bearing and air in the air gap. Therefore, the mechanical loss is proportional to the rotational speed. The measured mechanical loss can thus be modeled as a polynomial:

$$W_{mech} = c_0 + c_1 \cdot \omega_m + c_2 \cdot \omega_m^2 \quad (3)$$

where W_{mech} is the mechanical loss, ω_m is the rotational speed in rpm, and the c_n values are the polynomial coefficients. Figure 11a,b show a comparison of the loss and efficiency between the experiments and simulations at various rotational speeds. The total loss comprises the mechanical loss and the electromagnetic losses of the AC Joule loss, iron loss, eddy current loss of the PMs, and DC Joule loss of the end winding. Therefore, simulations were performed to calculate the electromagnetic losses under the rated torque and rotational speed. The mechanical loss was calculated using the fitted curve in Equation (3), and the eddy current loss of PMs was calculated using 3D transient analysis in order for considering the magnetic flux density of axial direction. The iron loss and total AC Joule loss were calculated using 2D transient analysis, and the AC Joule loss for each component was separated using the proposed method in Section 2.2. As the fundamental frequency increased, the AC Joule loss, iron loss, and eddy current loss of the PMs increased as well, and the mechanical loss was proportional to the rotational speed.

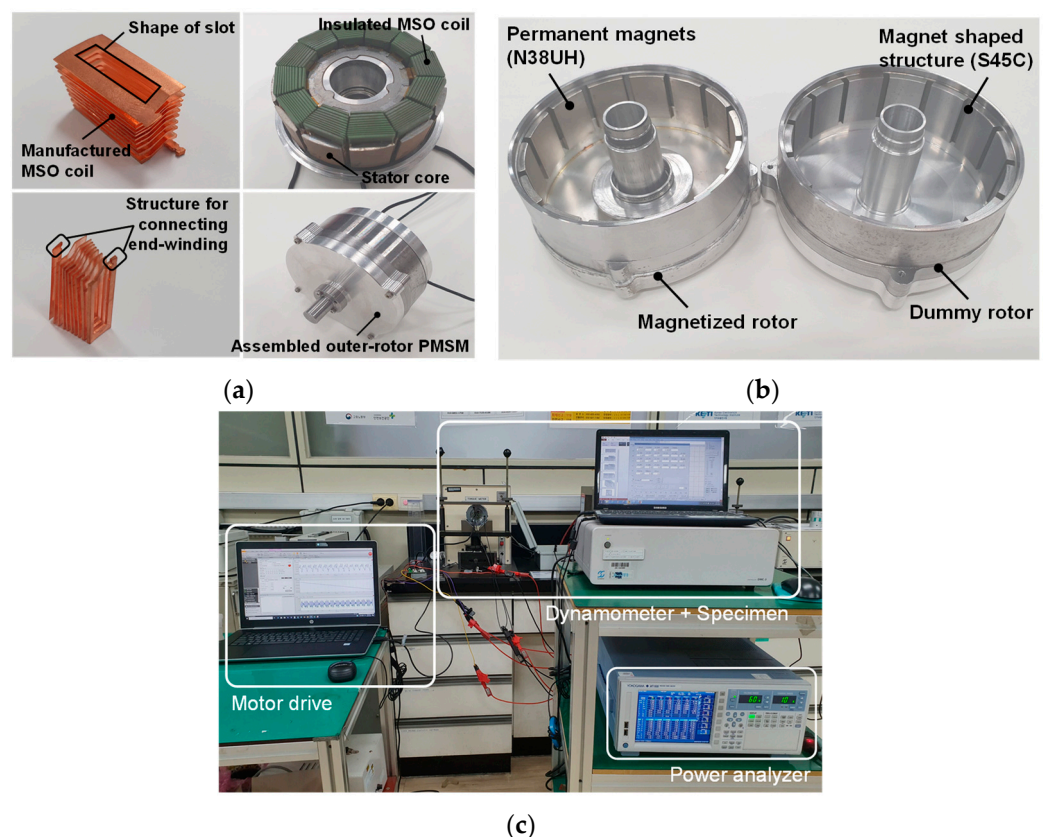


Figure 9. Specimen and experimental setup. (a) Manufactured specimen using MSO coil, (b) dummy rotor for measuring mechanical loss, and (c) experimental setup for verifying the specimen.

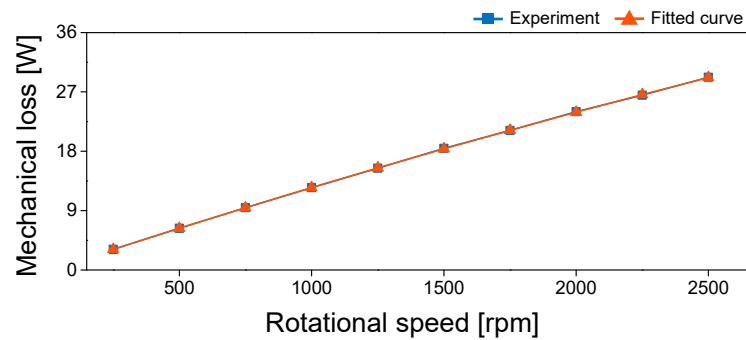


Figure 10. Experiment results for mechanical loss measurement.

Therefore, the total loss of the specimen increased with the rotational speed, as shown in Figure 11a. Because the pole and slot combination with the lowest AC Joule loss among the candidates was selected, the ratio of the AC Joule loss to the total loss decreased with increasing rotational speed. By using the total loss and output power at a given rotational speed, the efficiency of the specimen could be accurately predicted through simulations.

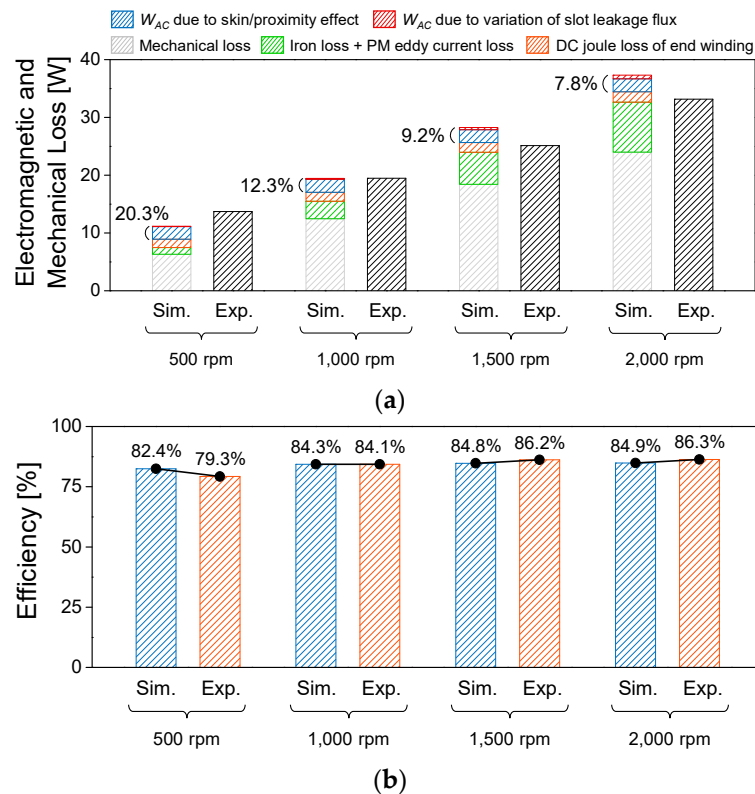


Figure 11. Comparison of experimental results with simulation results for (a) total loss and (b) efficiency.

5. Conclusions

A design guideline for selecting the pole and slot combination of an outer-rotor permanent magnet synchronous motor (PMSM) using a maximum slot occupation (MSO) coil was proposed. Because of the enlarged conductor area of the MSO coil, the AC Joule loss of conductors should be considered when designing a PMSM with an MSO coil. To analyze the effect of the number of poles and slots on the loss, a method for separating the loss due to each component was proposed. This method, which is effective in separating the eddy current by component, was usually used to separate the eddy current loss of permanent magnets. In this study, the method was used to separate the eddy current

loss of the conductors, and the trend of loss was compared according to the pole and slot combinations. The proposed method was verified using 2-D electromagnetic finite element analysis (FEA). Using the proposed method, it was found that the proportion of AC Joule loss due to variation in slot leakage flux increased with the number of rotor poles and stator slots. Among the analyzed models, the model with 14-poles and 12-slots had the lowest AC Joule loss. To verify the analysis results, the derived model was fabricated and verified through simulations and experiments.

Author Contributions: Conceptualization, S.-H.P. and M.-S.L.; methodology, S.-H.P.; software, S.-H.P. and G.-J.L.; validation, S.-H.P. and E.-C.L.; resources, E.-C.L. and S.-O.K.; writing—original draft preparation, S.-H.P.; writing—review and editing, E.-C.L. and G.-J.L.; visualization, E.-C.L.; supervision, M.-S.L.; project administration, S.-O.K.; funding acquisition, S.-O.K. All authors have read and agreed to the published version of the manuscript.

Funding: This research received no external funding.

Acknowledgments: This work was supported by the Safety System R&D Group, Korea Institute of Industrial Technology (KITECH). This work was supported by the National Research Foundation of Korea (NRF) grant funded by the Korea government (MSIT) (NRF-2020R1A4A4079701).

Conflicts of Interest: The authors declare no conflict of interest.

References

- Bolam, R.C.; Vagapov, Y.; Anuchin, A. A Review of Electrical Motor Topologies for Aircraft Propulsion. In Proceedings of the 2020 55th International Universities Power Engineering Conference (UPEC), Turin, Italy, 1–4 September 2020; IEEE: New York, NY, USA, 2020; pp. 1–6.
- Zhao, T.; Wu, S.; Cui, S. Multiphase PMSM With Asymmetric Windings for More Electric Aircraft. *IEEE Trans. Transp. Electrification* **2020**, *6*, 1592–1602. [[CrossRef](#)]
- Ehsani, M.; Gao, Y.; Miller, J.M. Hybrid Electric Vehicles: Architecture and motor drives. *Proc. IEEE* **2007**, *95*, 719–728. [[CrossRef](#)]
- Song, Z.; Liu, C.; Feng, K.; Zhao, H.; Yu, J. Field Prediction and Validation of a Slotless Segmented-Halbach Permanent Magnet Synchronous Machine for More Electric Aircraft. *IEEE Trans. Transp. Electrification* **2020**, *6*, 1577–1591. [[CrossRef](#)]
- Islam, M.S.; Husain, I.; Ahmed, A.; Sathyan, A. Asymmetric Bar Winding for High-Speed Traction Electric Machines. *IEEE Trans. Transp. Electrification* **2020**, *6*, 3–15. [[CrossRef](#)]
- Rahman, K.M.; Jurkovic, S.; Stancu, C.; Morgante, J.; Savagian, P.J. Design and Performance of Electrical Propulsion System of Extended Range Electric Vehicle (EREV) Chevrolet Volt. *IEEE Trans. Ind. Appl.* **2015**, *51*, 2479–2488. [[CrossRef](#)]
- Park, H.J.; Lim, M.S. Design of High Power Density and High Efficiency Wound-Field Synchronous Motor for Electric Vehicle Traction. *IEEE Access* **2019**, *7*, 46677–46685. [[CrossRef](#)]
- Berardi, G.; Bianchi, N. Design Guideline of an AC Hairpin Winding. In Proceedings of the 2018 XIII International Conference on Electrical Machines (ICEM), Alexandroupoli, Greece, 3–6 September 2018; IEEE: New York, NY, USA, 2018; pp. 2444–2450.
- Chin, J.W.; Cha, K.S.; Park, M.R.; Park, S.H.; Lee, E.C.; Lim, M.S. High Efficiency PMSM with High Slot Fill Factor Coil for Heavy-Duty EV Traction Considering AC Resistance. *IEEE Trans. Energy Convers.* **2020**. [[CrossRef](#)]
- Park, S.H.; Lee, E.C.; Park, J.C.; Hwang, S.W.; Lim, M.S. Prediction of Mechanical Loss for High Power Density PMSM Considering Eddy Current Loss of PMs and Conductors. *IEEE Trans. Magn.* **2021**, *57*, 1–5.
- Cha, K.S.; Chin, J.W.; Park, S.H.; Jung, Y.H.; Lee, E.C.; Lim, M.S. Design Method for Reducing AC Resistance of Traction Motor using High Fill Factor Coil to Improve Fuel Economy of eBus. *IEEE/ASME Trans. Mechatron.* **2021**. [[CrossRef](#)]
- Morisco, D.P.; Kurz, S.; Rapp, H.; Möckel, A. A Hybrid Modeling Approach for Current Diffusion in Rectangular Conductors. *IEEE Trans. Magn.* **2019**, *55*, 8002111. [[CrossRef](#)]
- Bianchi, N.; Berardi, G. Analytical Approach to Design Hairpin Windings in High Performance Electric Vehicle Motors. In Proceedings of the 2018 IEEE Energy Conversion Congress and Exposition (ECCE), Portland, OR, USA, 23–27 September 2018; pp. 4398–4405.
- Popescu, M.; Goss, J.; Staton, D.A.; Hawkins, D.; Chong, Y.C.; Boglietti, A. Electrical Vehicles—Practical Solutions for Power Traction Motor Systems. *IEEE Trans. Ind. Appl.* **2018**, *54*, 2751–2762. [[CrossRef](#)]
- Pyrhonen, J.; Jokinen, T.; Hrabovcov, V. Resistances. In *Design of Rotating Electrical Machines*, 1st ed.; Wiley: Oxford, UK, 2009.
- Kim, D.M.; Kim, J.H.; Lee, S.G.; Park, M.R.; Lee, G.H.; Lim, M.S. Estimation Method for Rotor Eddy Current Loss in Ultra-High-Speed Surface-Mounted Permanent Magnet Synchronous Motor. *IEEE Trans. Magn.* **2021**, *57*, 1–5.
- Kim, J.H.; Kim, D.M.; Jung, Y.H.; Lim, M.S. Design of Ultra-High-Speed Motor for FCEV Air Compressor Considering Mechanical Properties of Rotor Materials. *IEEE Trans. Energy Convers.* **2021**. [[CrossRef](#)]
- Chu, G.; Dutta, R.; Pouramin, A.; Rahman, M.F. Analysis of Torque Ripple of a Spoke-Type Interior Permanent Magnet Machine. *Energies* **2020**, *13*, 2886. [[CrossRef](#)]

-
19. Walker, J.A.; Dorrell, D.G.; Cossar, C. Flux-linkage calculation in permanent-magnet motors using the frozen permeabilities method. *IEEE Trans. Magn.* **2005**, *41*, 3946–3948. [[CrossRef](#)]
 20. Kim, H.J.; Jeong, J.S.; Yoon, M.H.; Moon, J.W.; Hong, J.P. Simple Size Determination of Permanent-Magnet Synchronous Machines. *IEEE Trans. Ind. Electron.* **2017**, *64*, 7972–7983. [[CrossRef](#)]